

LETTER • OPEN ACCESS

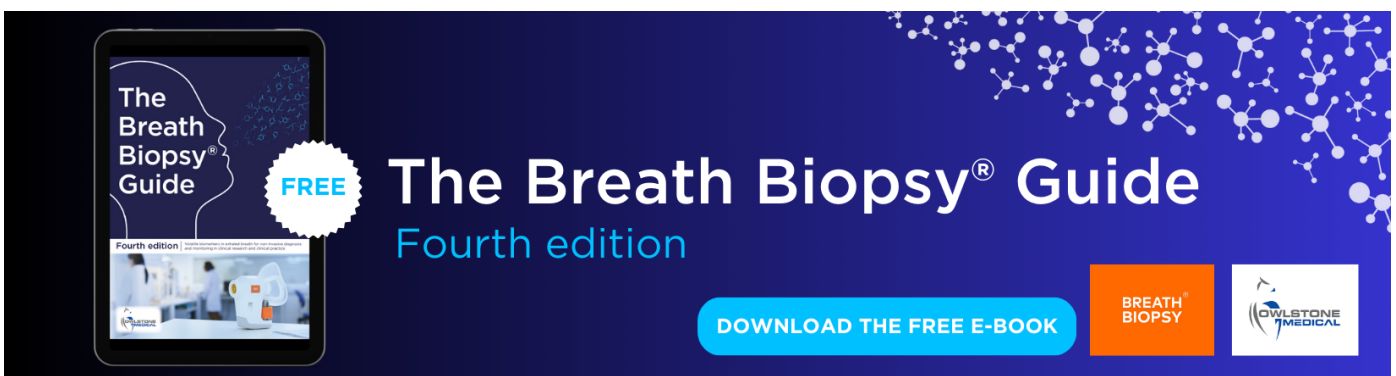
Analysis of variation in reference evapotranspiration and its driving factors in mainland China from 1960 to 2016

To cite this article: Dong Wu *et al* 2021 *Environ. Res. Lett.* **16** 054016

View the [article online](#) for updates and enhancements.

You may also like

- [Spatiotemporal patterns of evapotranspiration in response to multiple environmental factors simulated by the Community Land Model](#)
Xiaoying Shi, Jiafu Mao, Peter E Thornton *et al.*
- [Water use by terrestrial ecosystems: temporal variability in rainforest and agricultural contributions to evapotranspiration in Mato Grosso, Brazil](#)
Michael J Lathuilière, Mark S Johnson and Simon D Donner
- [Stomatal response to decreased relative humidity constrains the acceleration of terrestrial evapotranspiration](#)
Mingzhong Xiao, Zhongbo Yu, Dongdong Kong *et al.*



The Breath Biopsy® Guide
Fourth edition

FREE

DOWNLOAD THE FREE E-BOOK

BREATH BIOPSY

OWLSTONE MEDICAL

ENVIRONMENTAL RESEARCH
LETTERS

LETTER

Analysis of variation in reference evapotranspiration and its driving factors in mainland China from 1960 to 2016

OPEN ACCESS

RECEIVED
18 January 2021REVISED
6 April 2021ACCEPTED FOR PUBLICATION
9 April 2021PUBLISHED
22 April 2021

Original content from this work may be used under the terms of the [Creative Commons Attribution 4.0 licence](#).

Any further distribution of this work must maintain attribution to the author(s) and the title of the work, journal citation and DOI.

Dong Wu^{1,2} , Shibo Fang^{1,2}, Xingyuan Tong³, Lei Wang¹, Wen Zhuo¹, Zhifang Pei⁴, Yingjie Wu¹, Ju Zhang⁴ and Mengqian Li¹¹ State Key Laboratory of Severe Weather, Chinese Academy of Meteorological Sciences, Beijing 100081, People's Republic of China² Collaborative Innovation Center on Forecast and Evaluation of Meteorological Disasters, Nanjing University of Information Science & Technology, Nanjing 210044, People's Republic of China³ Nanjing University of Information Science & Technology, Nanjing 210044, People's Republic of China⁴ Chengdu University of Technology, Chengdu 610000, People's Republic of ChinaE-mail: dr.sbfang@163.com**Keywords:** reference evapotranspiration, spatiotemporal variation, abrupt change, driving factor, mainland ChinaSupplementary material for this article is available [online](#)**Abstract**

Understanding the variation in reference evapotranspiration (ET_o) is vital for hydrological cycles, drought monitoring, and water resource management. With 1507 meteorological stations and 130 radiation-measured stations, the annual and seasonal ET_o were calculated at each site from 1960 to 2016 in mainland China. The phenomenon of coefficient 'a' being less than 0.25 and coefficient 'b' being greater than 0.50 in the Angstrom–Prescott model occurred in almost the whole country, except for a small area of western and northeastern China. Moreover, the Xiao's method was more applicable to calculate the net longwave radiation (R_{nl}) and then improve the estimation accuracy of ET_o . The annual ET_o varied from 538.8 to 1559.8 mm and had a high-value center located in the plateau and desert of northwestern China and a low-value center located in Northeast China and near the Sichuan Basin. The spatial distribution of seasonal ET_o was roughly similar to that of annual ET_o , except for that in winter when ET_o was high in the south and low in the north. In mainland China, the annual ET_o decreased by 21.2 mm decade⁻¹ because of the declining sunshine duration before 1993 and increased by 21.1 mm decade⁻¹ due to the decreased relative humidity (RH) after 1993. Generally, the abrupt change of ET_o mainly occurred in the southern China rather than northern China (except for Qinghai Tibet Plateau). Basically, the dominant driving factors of annual and seasonal ET_o were RH and/or T_{max} after the abrupt change in most parts of China.

1. Introduction

Actual evapotranspiration (ET_a), as the nexus of the water and energy balances, is a combined process whereby water is lost from the soil surface by evaporation and from vegetation by transpiration, thus linking the soil, vegetation and atmosphere together in terrestrial ecosystems (Allen *et al* 1998). Moreover, ET_a is the crucial component of the hydrological cycle and climate system and is broadly applied in regional water resource assessments, drought monitoring and early warning, and evaluations of the water use efficiency of ecosystems (Hanasaki *et al* 2008, Anderson *et al* 2011, Yang *et al* 2015). Therefore, a suite of measurements or estimation methods have

been developed to quantify ET_a , including weighing lysimeters, eddy covariance, scintillometers, crop coefficient methods, and conservation of mass or energy methods (Norman *et al* 1995, Allen *et al* 1998, Bastiaanssen *et al* 1998, Yee *et al* 2015, Soubie *et al* 2016). However, observations of ET_a are not only costly but also have insufficient time series, and ET_a is strongly affected by surface characteristics (e.g. land cover and land change), climatic factors and the amount of available water, which constrain its applications in the aspect of climate change (Arnell and Liu 2001, McVicar *et al* 2012).

In contrast, the atmospheric evaporative demand (AED) represents the maximum evapotranspiration from a surface with an unlimited water supply

Table 1. Timing of abrupt change and major driving factors of annual ET_o analyzed with different data products in China.

Location	Period	Data	Abrupt change point	Driving factors	Source
Mainland China	1961–2013	0.5° gridded dataset	1982	U_2, T_{max}	Wang <i>et al</i> (2017)
Mainland China	1979–2015	0.1° gridded dataset	1990s	T	Wang <i>et al</i> (2019)
Mainland China	1956–2015	200 stations	1984	U_2/T_{min} & SD in subregions	Fan <i>et al</i> (2016)
Mainland China	1970–2014	598 stations	1993	T_{max}, T_{min}	Zhang <i>et al</i> (2019)
Three Gorges Reservoir	1960–2013	41 stations	1982	—	Lv <i>et al</i> (2016)
Southwest China	1961–2016	99 stations	1996	1961–1996: SD, U_2 1997–2016: RH, T	Jiang <i>et al</i> (2019)

Note: T = average temperature; T_{max} = maximum temperature; T_{min} = minimum temperature; U_2 = wind speed at a height of 2 m; SD = sunshine duration; RH = relative humidity of atmosphere.

under certain meteorological conditions, and it is mainly characterized by three indicators: potential evapotranspiration (ET_p), reference evapotranspiration (ET_o) and pan evaporation (ET_{pan}) (Fan and Thomas 2018, Xiang *et al* 2020). Among these metrics, ET_o and ET_{pan} are extensively investigated in terms of temporal variability and attribution analysis because the former is independent of crop type, crop development and management practices and the latter provides a measurement of actual AED; both these variables are comparable in disparate climatic regions worldwide (Allen *et al* 1998, Wang *et al* 2017, Fan and Thomas 2018). However, the consistency of the pan evaporation data is not high enough in China for the reason that the type of evaporation pan was changed from D20 pan to E601B around 2000 but the homogenization has not been applied to the data (Yang and Yang 2012, National Standard of People's Republic of China, GB/T35230-2017 2017). Many studies published at the beginning of the 21st century verified that most regions or countries, such as Australia, New Zealand, Alberta, the United States, China, and India, have suffered significant decreases in annual ET_{pan} or ET_o in the past 50 years (Chattopadhyay and Hulme 1997, Thomas 2000, Roderick and Farquhar 2002, Hobbins and Ramírez 2004, Xu *et al* 2006, Rayner 2007). Obviously, the aforementioned phenomenon conflicts with the projected capacity of the atmosphere to hold more water vapor as the air temperature increased by 0.74 °C during the 20th century (Roderick and Farquhar 2002, McVicar *et al* 2012). Further investigation of synchronous climate information indicated that decreases in wind speed (termed 'stilling') and/or radiation (termed 'dimming') offset warming, inducing a decline in the AED (Roderick and Farquhar 2002, McVicar *et al* 2012, Jahani *et al* 2017). This is a convincing interpretation because the variability in AED is affected by the interaction of multiple meteorological elements, especially wind speed, atmospheric humidity, radiation and air temperature.

In recent years, as the length of the time series of meteorological observations has been expanding, abrupt change in annual ET_o have been detected in some regions. In Greece, the abrupt change in annual ET_o occurred in the early 1980s; before the 1980s, ET_o decreased over time, while after the 1980s, it increased (Papaioannou *et al* 2011). In China, trend analyses have been implemented in different administrative, geographic and climatic regions, and monotonic and nonmonotonic changes have been reported in previous studies (Huo *et al* 2013, Lv *et al* 2016, Gao *et al* 2017, Wang *et al* 2019). For example, Wang *et al* (2016) depicted that the annual ET_o in the three-river source region decreased significantly by $-9.1 \text{ mm decade}^{-1}$ from 1980 to 2012; Wang *et al* (2019) showed that the annual ET_o first decreased and then increased in mainland China (MLC) based on the China Meteorological Forcing Dataset from 1979 to 2015. In addition, the timing of abrupt change of annual ET_o generally occurred in the 1980s or 1990s in China because existing studies were performed at disparate spatial scales (table 1). Synchronously, the dominant driving factors of annual ET_o have been extracted by various approaches, such as multiple linear regression, differentiation equations, and Gaussian geographic weighted regression models (Wang *et al* 2016, 2017, Gao *et al* 2017, Zhang *et al* 2019).

Reviewing the published literature, several shortcomings regarding the ET_o trend and its contributing factors must be addressed in MLC. First, strengthening the analysis of the seasonal ET_o pattern is necessary in light of the variability in meteorological elements in different seasons. Second, it should be noted that markedly disparate timing of abrupt change of annual ET_o was detected by several studies with the same spatial extent in MLC (table 1). Hence, it is crucial to adopt higher-quality data to further explore whether differences in data richness and data sources influence the assessment results. Finally, it is not clear whether the main driving factors of the ET_o sequence change before and after the abrupt change.

Consequently, the objectives of this study were to (a) analyze the spatial distribution of annual and seasonal ET_o in MLC from 1960 to 2016; (b) investigate the annual and seasonal ET_o series and determine the corresponding abrupt change points based on observations from higher-density meteorological stations; and (c) implement attribution analysis to explore the dominant driving factors of ET_o before and after the abrupt change. The results are expected to serve as a reference for the evaluation of crop water demand, drought risk assessment and water resource allocation in MLC.

2. Data and methodology

2.1. Study area

China, the third largest country in the world, is characterized by various and complicated climates (e.g. temperate monsoon climate, temperate continental climate, subtropical monsoon climate, tropical monsoon climate and plateau alpine climate) and geographies (e.g. plain, plateau, basin, hill and mountain). Based on the specific combinations of climatic resources and terrains, MLC can be divided into nine agricultural regions, including the North-east China Plain (I), northern arid and semiarid region (II), Huang-Huai-Hai Plain (III), Loess Plateau (IV), Qinghai Tibet Plateau (V), Sichuan Basin and surrounding regions (VI), middle-lower Yangtze Plain (VII), Yunnan-Guizhou Plateau (VIII), and southern China (IX) (figure 1(a), www.resdc.cn/data.aspx?DATAID=275). The multiyear averaged conditions of climatic elements are summarized in table S1 (available online at stacks.iop.org/ERL/16/054016/mmedia) for each region.

2.2. Data sources and processing

The daily meteorological observation data of 1507 high-density synoptic sites (figure 1(b)) were collected by the National Meteorological Information Centre of the China Meteorological Administration (<http://data.cma.cn>) from 1960 to 2016, consisting of average temperature (T), maximum temperature (T_{max}), minimum temperature (T_{min}), wind speed at a height of 10 m (U_{10}), relative humidity (RH), sunshine duration (SD), and precipitation (Pre). Moreover, 130 radiation-measured sites recorded the surface net radiation (R_n) and shortwave radiation received (R_s) and reflected (R_{ref}) by the surface (only a few sites measured all elements) and were evenly distributed in MLC (figure 1(b)). However, the available number of radiation-measured sites varied over time because some of the stations had missing observations in certain years (figure S1).

An entire year is separated into four seasons: spring (March–May), summer (June–August), autumn (September–November) and winter (December–February). To estimate the relevant

parameters during different seasons, screening criteria were adopted; for example, if a meteorological element is completely missing in a season, the relevant data for that season is no longer used. And the percentage of missing data against the entire sequence from 1960 to 2016 was controlled within 3.5% for each climatic factor. Subsequently, two gap-filling methods were implemented for the time series of climatic factors: (a) linear interpolation was used when the number of continuous missing data points was less than 5, and these missing values were substituted with the mean value of other years when the number of continuous missing data points was greater than 4 for all climatic factors except for precipitation; and (b) replacement with the value on the same day from the nearest meteorological stations was used for only the precipitation data (Wu *et al* 2019).

2.3. Estimation of ET_o

In this study, the FAO (Food and Agriculture Organization of the United Nations) Penman–Monteith equation was employed to calculate the daily ET_o with basic meteorological parameters, which were defined as a hypothetical grass surface with a crop height of 0.12 m, a fixed surface resistance of 70 s m^{-1} , an albedo of 0.23, and an adequate water supply (Allen *et al* 1998). The formula is expressed as follows:

$$ET_o = \frac{0.408\Delta(R_n - G) + \gamma \frac{900}{T+273} U_2 (e_s - e_a)}{\Delta + \gamma(1 + 0.34U_2)} \quad (1)$$

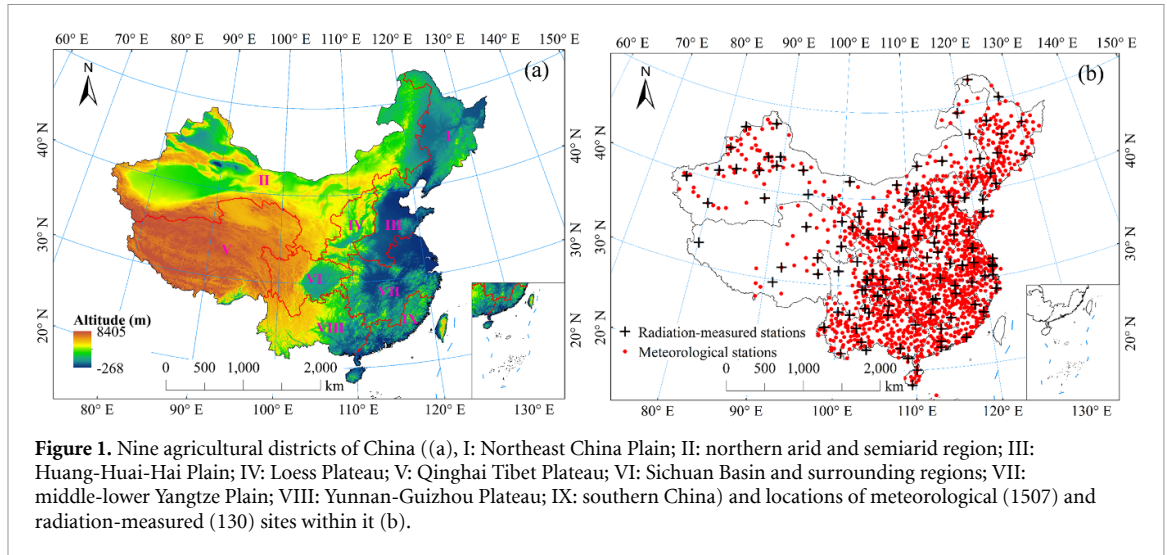
where ET_o is the daily reference evapotranspiration (mm d^{-1}); Δ is the slope of the saturated vapor pressure curve ($\text{kPa } ^\circ\text{C}^{-1}$); γ is the psychrometric constant ($\text{kPa } ^\circ\text{C}^{-1}$); e_s is the saturation vapor pressure (kPa); e_a is the actual vapor pressure (kPa); T is the mean air temperature ($^\circ\text{C}$) at a 2 m height, which is computed as the mean of T_{max} ($^\circ\text{C}$) and T_{min} ($^\circ\text{C}$); G is the soil heat flux ($\text{MJ m}^{-2} \text{ d}^{-1}$) and is so small that it can be ignored for a one-day period; and U_2 is the wind speed at a height of 2 m (m s^{-1}), and a logarithmic wind speed profile relationship is capable of converting U_{10} to U_2 (Allen *et al* 1998):

$$U_2 = U_{10} \frac{4.87}{\ln(67.8z - 5.42)} \quad (2)$$

where U_{10} is the measured wind speed at a height of 10 m, and z is the height of the measurement above the ground surface (i.e. 10 m). R_n is the net radiation at the canopy surface ($\text{MJ m}^{-2} \text{ d}^{-1}$), which is the difference between net solar shortwave radiation (R_{ns} , $\text{MJ m}^{-2} \text{ d}^{-1}$) and net longwave radiation (R_{nl} , $\text{MJ m}^{-2} \text{ d}^{-1}$) (Allen *et al* 1998):

$$R_n = R_{ns} - R_{nl} \quad (3)$$

$$R_{ns} = (1 - \alpha) R_s \quad (4)$$



$$R_s = \left(a + b \frac{n}{N} \right) R_a \quad (5)$$

$$R_{nl} = \sigma \frac{T_{\max}^4 + T_{\min}^4}{2} (c + d\sqrt{e_a}) \left(f + (1-f) \frac{R_s}{R_{so}} \right) \quad (6)$$

where α is the albedo or canopy reflection coefficient, which is 0.23 for hypothetical reference grass; R_s is the solar shortwave radiation ($\text{MJ m}^{-2} \text{d}^{-1}$); n is the actual sunshine duration (i.e. SD, h); R_a , R_{so} and N are the extraterrestrial radiation ($\text{MJ m}^{-2} \text{d}^{-1}$), clear-sky solar radiation ($\text{MJ m}^{-2} \text{d}^{-1}$) and the maximum possible duration of sunshine (h), which are calculated by equations (21), (36) and (34) in FAO paper 56, respectively; σ is Stefan-Boltzmann constant ($4.903 \times 10^{-9} \text{ MJ K}^{-4} \text{ m}^{-2} \text{ d}^{-1}$); T_{\max} and T_{\min} are the maximum and minimum absolute air temperatures ($K = ^\circ\text{C} + 273.16$); and a , b , c , d and f are empirical regression coefficients (dimensionless), of which default values are 0.25, 0.50, 0.34, -0.14 , and -0.35 , respectively, recommended by FAO paper 56.

The ‘ a ’ and ‘ $a + b$ ’ variables represent the fraction of extraterrestrial radiation reaching the earth on overcast days and on clear days, respectively. Coefficients a and b change depending on atmospheric conditions and solar declination (Allen *et al* 1998). The vast extent, diverse climate and complex terrain in China may have a significant effect on the values of coefficients a and b . Consequently, the transformation of the Angstrom–Prescott model (i.e. equation (5)) was used to estimate ‘ a ’ and ‘ b ’ by the least square method:

$$\left(\frac{R_s}{R_a} \right) = a + b \left(\frac{n}{N} \right) \quad (7)$$

where R_s and n are the observations from the radiation-measured stations; and R_a is extraterrestrial radiation; and N is maximum sunshine hours. Here, (R_s/R_a) and (n/N) are the dependent and independent variables, respectively. Then, the coefficients ‘ a ’

and ‘ b ’ were estimated using the daily radiation data for each season from each available radiation-measured station from 1960 to 2016. Besides, different methods (i.e. different combinations of coefficients c , d and f) to estimate R_{nl} have great effects on ET_o (Yin *et al* 2008, Xiao and Kong 2021). In addition to equation (6), another basic form to simulate R_{nl} is as follow (Penman 1948, Doorenbos and Pruitt 1977, Xiao and Kong 2021):

$$R_{nl} = \sigma \frac{T_{\max}^4 + T_{\min}^4}{2} (c + d\sqrt{e_a}) \left(f + (1-f) \frac{n}{N} \right) \quad (8)$$

for the empirical coefficients in equation (8), a series of reference values (table 2) have been provided by Penman (1948), Doorenbos and Pruitt (1977) and Xiao and Kong (2021) based on observations. And we tried to compare these methods with R_{nl} observation in order to acquire the best R_{nl} model. The actual R_{nl} is calculated as follow (Xiao and Kong 2021):

$$R_{nl} = (R_s - R_{ref}) - R_n \quad (9)$$

where R_s , R_n and R_{ref} ($\text{MJ m}^{-2} \text{d}^{-1}$) are observations from radiation-measured stations, of which R_{ref} is the reflected solar radiation by the surface. Subsequently, daily ET_o could be computed based on climatic factors, the optimal R_{nl} model and the corresponding coefficients ‘ a ’ and ‘ b ’ derived from the nearest radiation-measured stations. And mean values of ET_o from all meteorological stations within a certain region were used to represent the regional conditions.

2.4. Trend detection

The nonparametric Mann–Kendall test was adopted to quantify the trend of ET_o at a prescribed significance level of α because its application is not limited by the distribution of sample data (Hirsch and Slack 1984, Dinpashoh *et al* 2011,

Table 2. Methods to calculate the net longwave radiation.

Expression	Name	c	d	f	Source
Equation (6)	FAO56	0.34	−0.14	−0.35	Allen <i>et al</i> (1998)
Equation (8)	Penman	0.56	−0.25	0.1	Penman (1948)
Equation (8)	FAO24	0.34	−0.14	0.1	Doorenbos and Pruitt (1977)
Equation (8)	Xiao	0.43	−0.15	0.36	Xiao and Kong (2021)

Jhajharia *et al* 2012). Note that the pre-whitening process for the ET_o time series was implemented first to avoid the impact of serial correlation of the sample on the Mann–Kendall trend test (Yue and Wang 2002). Additionally, the nonparametric Sen's slope estimator, developed by Sen, was used to evaluate the slope of the trend of a time series (Sen 1968). In the study, the significance level α of the Mann–Kendall trend test was set to 0.05 or 0.01. For the standard normal test statistic, Z , a significant ascending trend exists in the time series if Z is greater than 1.96 or 2.58, and a significant descending trend exists in the time series if Z is less than -1.96 or -2.58 .

Influenced by natural or anthropogenic factors, the variability of hydrological and meteorological time series are often periodic or oscillating but seldom monotonous (She *et al* 2017). The moment that the trend of the time series changes from increasing (decreasing) to decreasing (increasing) is termed abrupt change (Villarini *et al* 2012, Gu *et al* 2017). The Mann–Kendall abrupt test was widely applied to detect the abrupt change points of time series in the field of hydrology and meteorology (Yang and Tian 2009, Liang *et al* 2010, Zhao *et al* 2014). However, the Mann–Kendall abrupt test may induce the phenomenon of multiple abrupt change points (Fang *et al* 2016, Wu *et al* 2019). Therefore, the non-parametric Pettitt approach was employed to implement abrupt change analysis for the reason that it can identify one change point at a time (Pettitt 1979, Zuo *et al* 2012, Lv *et al* 2016, Wang *et al* 2016).

2.5. Multiple standardized stepwise regression

ET_o , which consists of radiative and aerodynamic terms, is comprehensively affected by diverse climatic factors, such as T , U_2 , SD , and RH , among which complex direct or indirect relationships exist. Moreover, the contribution of a specific climatic factor to ET_o depends on not only the sensitivity of ET_o but also its degree of change (Zhao *et al* 2020). To extract the dominant driving factors of annual or seasonal ET_o , a multiple standardized stepwise regression model was employed to establish the relation between dependent variables (i.e. ET_o) and independent variables (i.e. T_{max} , T_{min} , U_2 , RH , and SD) (Wang *et al* 2017). Specifically, the analysis process included: (a) normalizing the climatic factors and ET_o (with the mean and variance equal

to 0 and 1, respectively); (b) setting the maximum p value and minimum p value to 0.05 for an independent variable to be added to and removed from the linear model, respectively; (c) implementing the model fitting with MATLAB R2014a and R square representing the model performance; and (d) calculating the ratio of the regression coefficient of each independent variable against the sum of all the regression coefficients as the relative contribution of the climatic factor to ET_o ; the larger the contribution rate is, the more significant the climatic variable to ET_o is, and vice versa (Wang *et al* 2017).

2.6. Evaluation metrics

The coefficients of variation (CV) is used to depict the temporal variability of the relevant elements. The variability levels were limited by $CV \leq 0.1$, $0.1 < CV < 1.0$ and $CV \geq 1.0$, as weak, moderate and strong, respectively (Ayantobo *et al* 2017).

The performance of the R_{nl} models reported in table 2 were evaluated by the correlation coefficient (R), mean bias error (MBE) and root mean square error (RMSE) of the simulated values to measured values. The smaller the RMSE, the more accuracy of the R_{nl} model. MBE represent the estimation error, positive and negative means higher and lower estimation, respectively (Itenfisu *et al* 2003, Yin *et al* 2008). The R , MBE and RMSE were given by:

$$R = \frac{\sum_{i=1}^n (S_i - \bar{S})(O_i - \bar{O})}{\sqrt{\sum_{i=1}^n (S_i - \bar{S})^2 \sum_{i=1}^n (O_i - \bar{O})^2}} \quad (10)$$

$$MBE = \frac{\sum_{i=1}^n (S_i - O_i)}{n} \quad (11)$$

$$RMSE = \sqrt{\frac{\sum_{i=1}^n (S_i - O_i)^2}{n}} \quad (12)$$

where S_i and O_i are simulated and observed values of the i th sample, respectively; \bar{S} and \bar{O} are the mean values of simulated and observed samples, respectively; and n is the sample size.

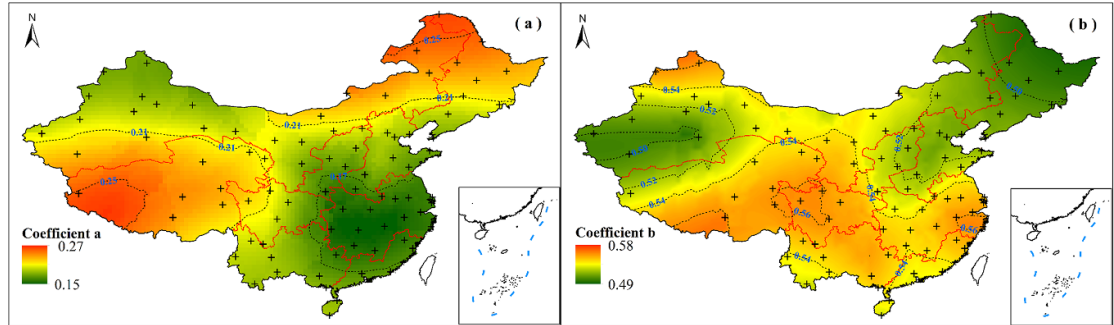


Figure 2. Spatial characteristics of coefficients ‘a’ (a) and ‘b’ (b) in the Angstrom-Prescott model for mainland China (calculated from 2000 to 2015 with 87 radiation-measured sites).

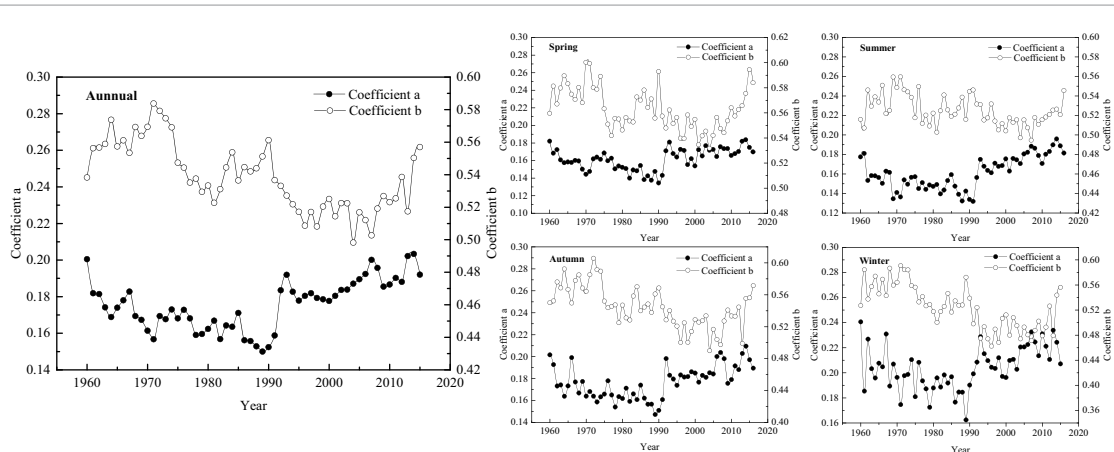


Figure 3. Annual and seasonal variability of coefficients ‘a’ and ‘b’ in the Angstrom–Prescott model in mainland China from 1960 to 2016.

3. Results

3.1. Spatiotemporal variability of coefficients ‘a’ and ‘b’ in the Angstrom–Prescott model

3.1.1. Spatial distribution of coefficients ‘a’ and ‘b’

The multiyear average of coefficients ‘a’ and ‘b’ in the Angstrom–Prescott model, based on the seasonal fitted values, was calculated for 87 radiation-measured stations from 2000 to 2015 (relatively more stations were available within the period). Then, the ordinary kriging method was adopted to interpolate the ‘a’ and ‘b’ coefficients and analyze the spatial heterogeneity in MLC (figure 2).

In most parts of MLC, coefficient ‘a’ was lower than 0.25, except in the northern zone I, northeastern zone II and western zone V (figure 2(a)). The stripes extending from Northeast China to Western China and extending from Southeast China to Northwest China were roughly viewed as the high-value and low-value regions of coefficient ‘a’, respectively. Furthermore, the whole middle-lower Yangtze Plain presented almost the lowest value of coefficient ‘a’, with a value less than 0.19 (figure 2(a)).

In most parts of MLC, coefficient ‘b’ was greater than 0.50, except in northeastern China and western zone II (figure 2(b)). The subregion, constituted by

zones I, II, III, and IV, had a coefficient ‘b’ below 0.54. However, coefficient ‘b’ in the rest of MLC was greater than 0.54. In addition, several high-value centers appeared in the northwestern zone II, southwestern zone V, western zone VI, and southeastern zone VII, with coefficient ‘b’ values greater than 0.56 (figure 2(b)).

3.1.2. Temporal variation in coefficients ‘a’ and ‘b’

Limited by the continuity of radiative data records, the temporal variation in coefficients ‘a’ and ‘b’ was analyzed from only 18 radiation-measured stations evenly distributed throughout MLC (figure S2). The annual and seasonal patterns of coefficient ‘a’ showed an approximately slight downward trend from 1960 to 1990, followed by an upward trend from 1990 to 2016 (figure 3). The multiyear average of seasonal coefficient ‘a’ gradually increased from spring (and summer) to winter (0.16, 0.16, 0.18, and 0.20 in sequence), and low variability with a coefficient (CV) less than 0.10 was present in each season (table 3). The annual and seasonal coefficient ‘b’ fluctuated and decreased from 1960 to approximately 2005 but increased slightly in recent years (figure 3). Coefficient ‘b’ was largest in spring, with a multiyear average of 0.56, followed by that in autumn, summer

Table 3. Annual and seasonal statistics on coefficients 'a' and 'b' in the Angstrom–Prescott model in mainland China from 1960 to 2016 (CV denotes the coefficient of variation).

Seasons	Coefficient 'a'				Coefficient 'b'				Correlation	p
	Max.	Min.	Mean	CV	Max.	Min.	Mean	CV		
Annual	0.20	0.15	0.18	0.08	0.58	0.50	0.54	0.04	−0.46	<0.01
Spring	0.18	0.13	0.16	0.08	0.60	0.53	0.56	0.03	−0.30	0.02
Summer	0.20	0.13	0.16	0.10	0.56	0.49	0.52	0.03	−0.55	<0.01
Autumn	0.21	0.15	0.18	0.09	0.61	0.49	0.54	0.05	−0.45	<0.01
Winter	0.24	0.16	0.20	0.08	0.59	0.46	0.52	0.07	−0.51	<0.01

Table 4. Validation stations for net longwave radiation used in the study.

No.	ID	Station	Province	Latitude (°E)	Longitude (°E)	Elevation (m)	Sample size (day)
1	54511	Beijing	Beijing	39.80	116.47	31.3	8724
2	52889	Lanzhou	Gansu	36.05	103.88	1517.2	4356
3	52983	Yuzhong	Gansu	35.87	104.15	1874.4	4314
4	59287	Guangzhou	Guangzhou	23.22	113.48	70.7	8712
5	57816	Guiyang	Guizhou	26.58	106.73	1223.8	1594
6	59948	Sanya	Hainan	18.22	109.58	419.4	8669
7	57083	Zhengzhou	Henan	34.72	113.65	110.4	8729
8	50136	Mohe	Heilongjiang	52.97	122.52	438.5	7044
9	50953	Haerbing	Heilongjiang	45.93	126.57	118.3	8724
10	57494	Wuhan	Hubei	30.60	114.05	23.6	8629
11	54342	Shenyang	Liaoning	41.73	123.52	49.0	8620
12	52267	Ejinaqi	Neimenggu	41.95	101.07	940.5	8709
13	52818	Geermu	Qinghai	36.42	94.92	2807.6	8655
14	58362	Baoshan	Shanghai	31.4	121.45	5.5	8668
15	51463	Urumqi	Xinjiang	43.78	87.65	935.0	8599
16	51709	Kashi	Xinjiang	39.48	75.75	1385.6	8642
17	57516	Shapingba	Chongqing	29.58	106.47	259.1	29

and winter. A smaller variability (CV below 0.07) existed in the four seasons compared to that of coefficient 'a'. Moreover, a significantly moderate negative correlation was detected between coefficients 'a' and 'b' at different time scales (table 3). One of the main reasons for this result is that the sum of coefficients 'a' and 'b' is constrained to less than 1.

3.2. Comparison of estimation methods of R_{nl}

Seventeen radiation-measured stations in MLC were selected to analyse the applicability of the four estimation methods of R_{nl} because of R_s , R_n and R_{ref} were observed in these sites. Table 4 depicted the site locations and sample size of the observations. The actual R_{nl} could be obtained by equation (9) and the most suitable R_{nl} model could be extracted by means of analysis of relevant statistical indicators.

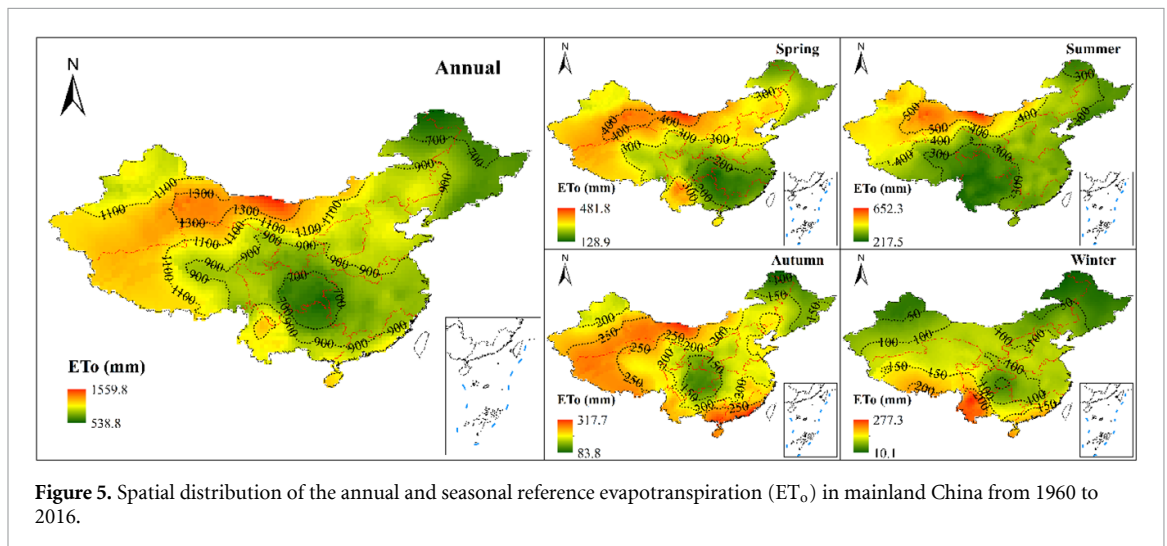
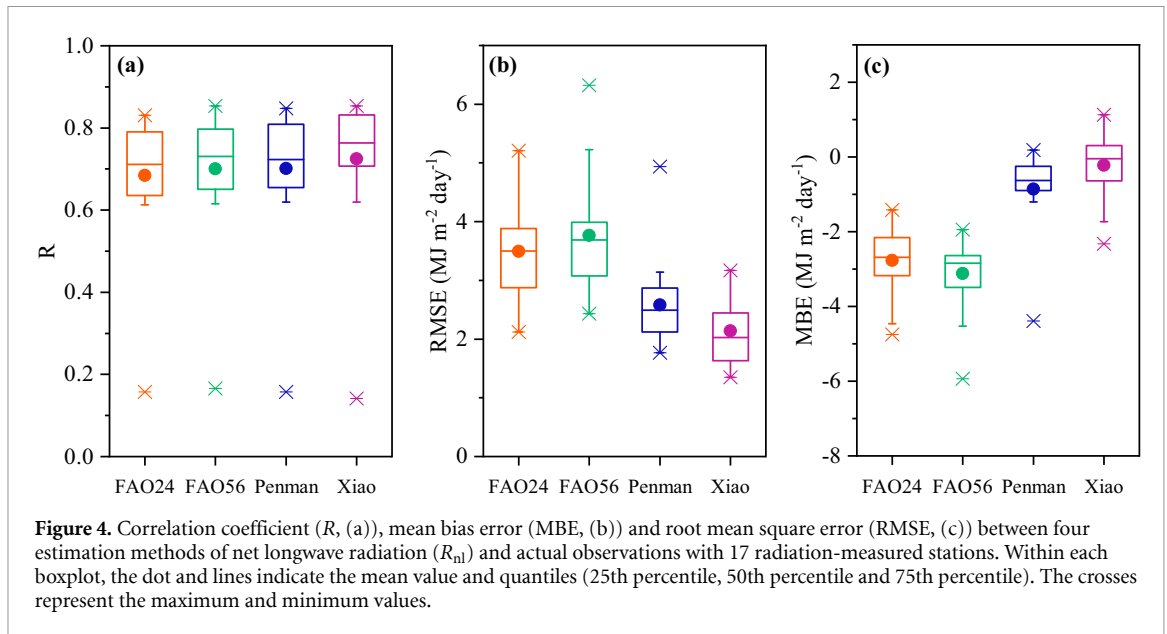
The correlations between four R_{nl} methods and actual observations were basically similar, of which Xiao's method had a slightly stronger relationship with observations (i.e. mean value of R was 0.73 within 17 sites) (figure 4(a)). Moreover, the accuracy of R_{nl} simulation by FAO56 and FAO24 was extremely low and the RMSE were 3.77 and 3.49 $\text{MJ m}^{-2} \text{d}^{-1}$, respectively. However, the estimation methods of R_{nl} developed by Penman and Xiao could calculate the net longwave radiation well and Xiao's method

had the highest accuracy with RMSE equal to 2.14 $\text{MJ m}^{-2} \text{d}^{-1}$ (figure 4(b)). In addition, estimation methods of R_{nl} by FAO56 and FAO24 completely underestimated the net longwave radiation on the 17 stations and the mean values of MBE were -3.12 and $-2.77 \text{ MJ m}^{-2} \text{d}^{-1}$, respectively. Nevertheless, the mean value of MEB between simulated R_{nl} by Xiao's method and observations was approximately close to 0 (MBE was equal to $-0.22 \text{ MJ m}^{-2} \text{d}^{-1}$) (figure 4(c)). In conclusion, Xiao's method had a high accuracy to estimate R_{nl} and was employed to compute ET_o as a crucial sub procedure in the study.

3.3. Spatiotemporal variability of ET_o

3.3.1. Annual and seasonal patterns of the spatial distribution of ET_o

The multiyear average annual ET_o ranged from 538.8 to 1559.8 mm in MLC. Generally, the inland ET_o in the northwest was higher than that in the central and eastern parts of China. The high-value region with an ET_o above 1100 mm mainly presented in the central and western parts of zone II and the western part of zone V, where the plateau and Gobi Desert are located. The low-value regions with an ET_o below 700 mm were located in the northeastern part of the MLC and adjacent areas among zone VI, zone VII and zone VIII (figure 5).



The spatial distribution of ET_0 in spring, summer and autumn was basically similar to its annual pattern, except for the magnitude of ET_0 , the slightly shifted location and the diverse extent of high-value and low-value regions. For example, the locations of the relatively low- ET_0 region varied from South China (surrounded by a 200 mm contour) to Southwest China (surrounded by a 300 mm contour) to Central China (surrounded by a 150 mm contour). However, an obvious graded distribution of ET_0 was present in winter, gradually increasing from Northwest and Northeast China to Southwest China. Overall, the ET_0 was largest in summer, followed by that in spring, autumn, and winter (figure 5).

3.3.2. Temporal variation in ET_0 and its abrupt change
An abrupt change point that occurred in 1993 was detected in the time sequence of the annual ET_0 from 1960 to 2016 in MLC; before this point, the annual ET_0 decreased by $21.2 \text{ mm decade}^{-1}$, while after

this point, the values displayed an increasing trend of $21.1 \text{ mm decade}^{-1}$ (figures 6 and 8). Moreover, the ET_0 sequences during spring and summer were also separated into an increasing and a decreasing segments due to the abrupt change, and the timing of these abrupt change points were 2004 and 1996, respectively (figures 6 and 7). Compared with the ET_0 time series in summer, the ET_0 sequence in spring decreased more slowly before abrupt change and increased more faster after abrupt change (figure 8). However, there were no abrupt change points for the ET_0 sequences during autumn and winter and the insignificant increased trends were detected with 0.6 and $1.0 \text{ mm decade}^{-1}$, respectively (figure 8).

Generally, the abrupt change had not been detected for most annual and seasonal ET_0 time series in northern China, such as zone I, zone II, zone III and zone IV (except for zone V) (figure 7). However, a majority of the annual and seasonal ET_0 time series in the Qinghai Tibet Plateau (i.e. zone

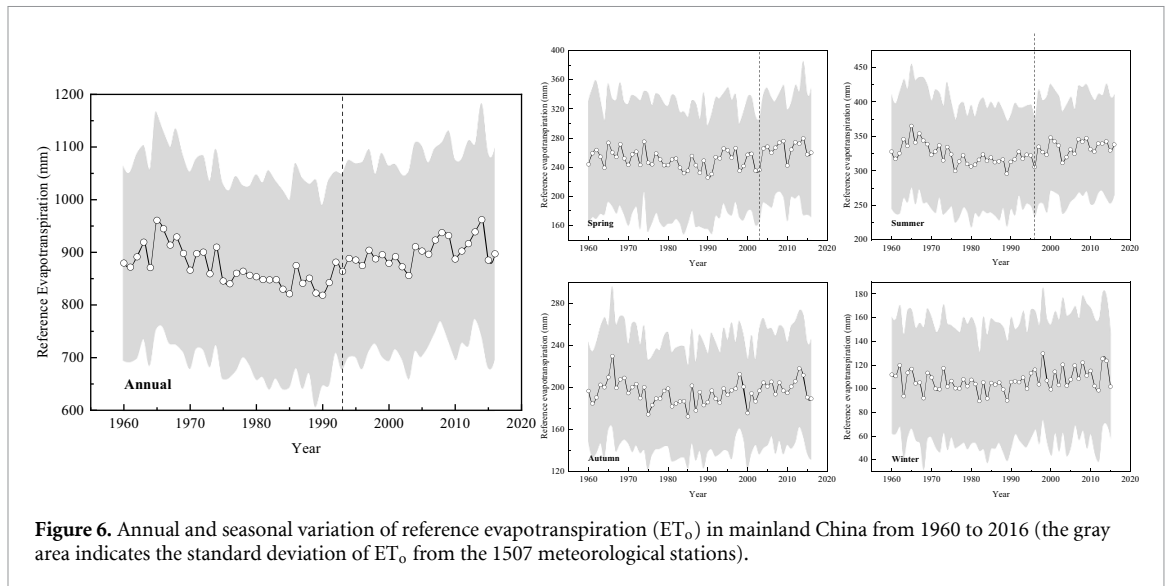


Figure 6. Annual and seasonal variation of reference evapotranspiration (ET_0) in mainland China from 1960 to 2016 (the gray area indicates the standard deviation of ET_0 from the 1507 meteorological stations).

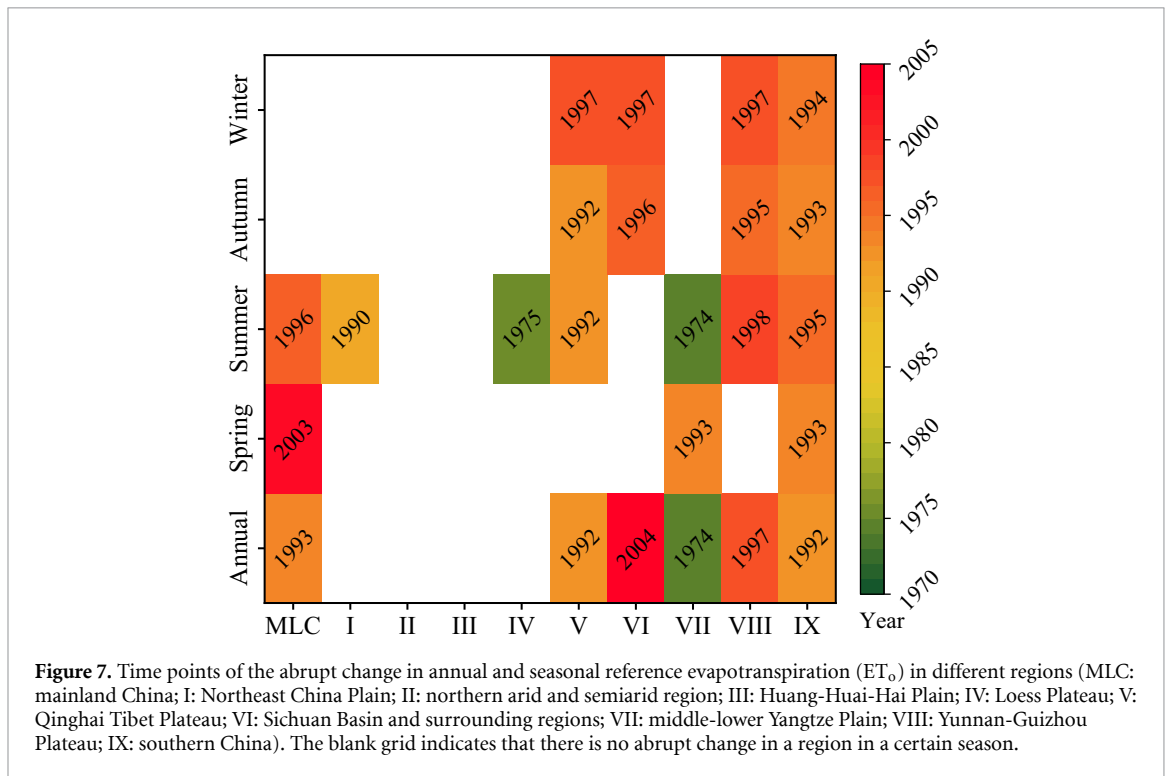


Figure 7. Time points of the abrupt change in annual and seasonal reference evapotranspiration (ET_0) in different regions (MLC: mainland China; I: Northeast China Plain; II: northern arid and semiarid region; III: Huang-Huai-Hai Plain; IV: Loess Plateau; V: Qinghai Tibet Plateau; VI: Sichuan Basin and surrounding regions; VII: middle-lower Yangtze Plain; VIII: Yunnan-Guizhou Plateau; IX: southern China). The blank grid indicates that there is no abrupt change in a region in a certain season.

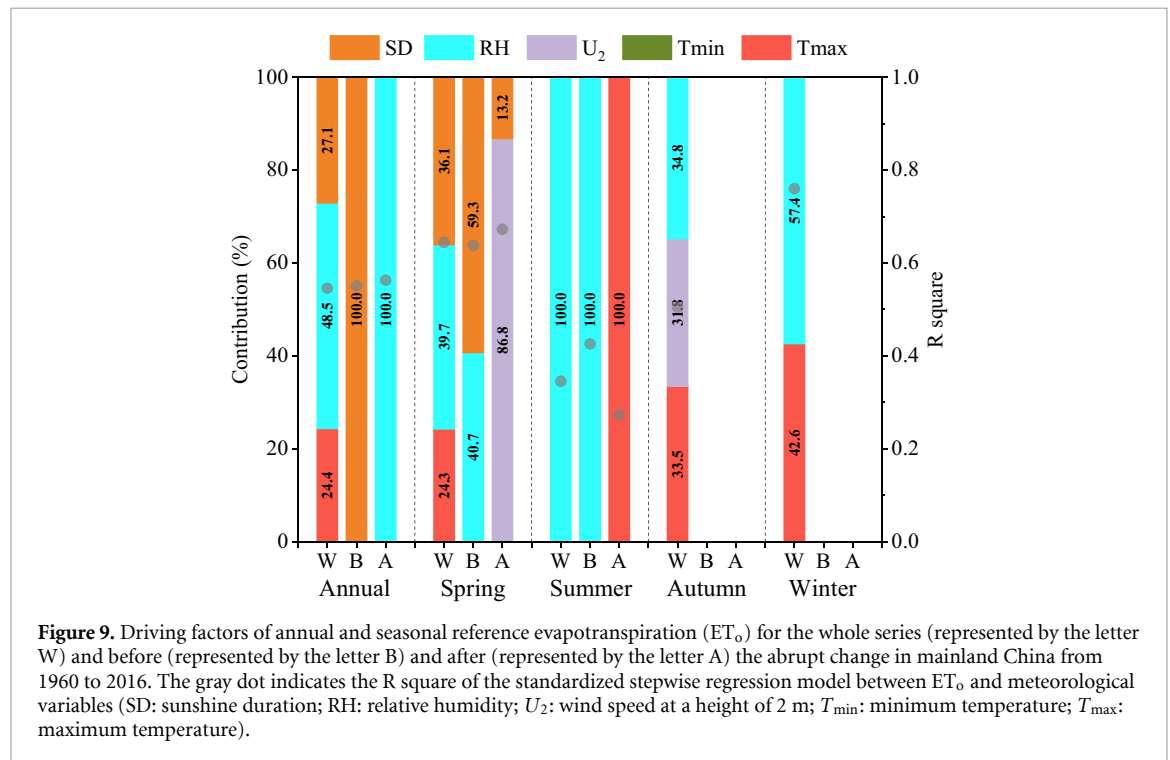
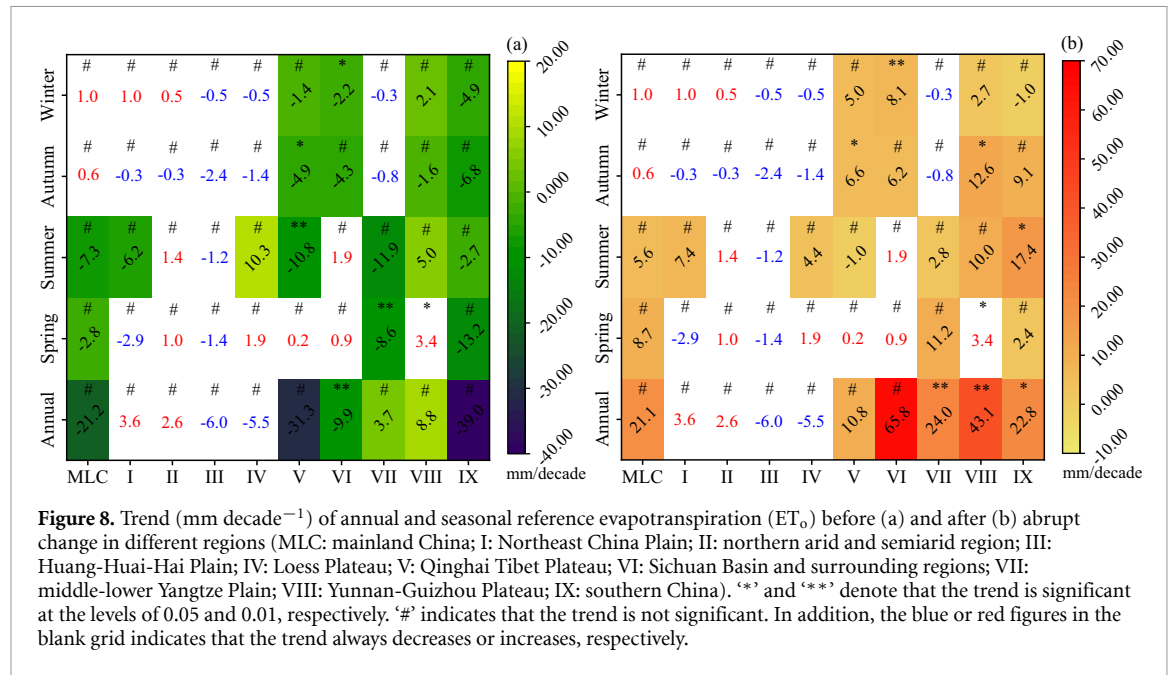
V) and the southern China were disturbed by the abrupt change, which caused a descending sequence and a subsequent ascending sequence (figures 7 and 8). The timing of the abrupt change of the annual ET_0 sequence in subregions was particularly early or late, such as that in zone VII, which had an abrupt change point appearing in 1974, and that in zone VI, which had an abrupt change point appearing in 2004. However, the abrupt change of the seasonal ET_0 time series generally occurred in approximately 1995, especially in autumn and winter (figure 7).

The annual ET_0 in zone I and II and zone III and IV continuously but insignificantly increased or declined. Moreover, the annual ET_0 in zone V and

IX decreased by more than $30 \text{ mm decade}^{-1}$ before abrupt change, which was higher than that in MLC. And the annual ET_0 in zone VI and VIII increased by more than $40 \text{ mm decade}^{-1}$ after abrupt change, which was far larger than in MLC or other subregions. Basically, the decrease in ET_0 in summer and the increase in ET_0 in summer and autumn played important roles in the corresponding trend of the annual ET_0 before and after the abrupt change in most subregions (figure 8).

3.4. Driving factors of annual and seasonal ET_0

The annual ET_0 in MLC was regulated by RH, SD and T_{max} , which contributed 48.5%, 27.1%, and 24.4%, respectively, to the variability in ET_0 from 1960 to



2016. However, the driving factors of annual ET_0 were completely disparate before and after the abrupt change, which were SD and RH respectively. For the whole seasonal ET_0 , the RH was the dominant driving factor in spring, summer, autumn, and winter, and the contributions were 39.7%, 100%, 34.8%, and 58.7%, respectively. Furthermore, the driving factors of seasonal ET_0 before and after abrupt change during spring and summer were completely disparate. Before abrupt change, the seasonal ET_0 were mainly affected by SD and RH in spring and summer, respectively. However, the dominant driving factors were U_2 and

T_{\max} after abrupt change in spring and summer, respectively (figures 9 and 10).

Affected by diverse climates and complex terrains, the drivers of annual and seasonal ET_0 were significantly distinct in the different subregions. For the annual ET_0 in each subregion, the RH in southern China (zone VI, VII, VIII, and IX) and zone II and IV, the T_{\max} in zone I and V, and the U_2 in zone III were the corresponding dominant driving factors of ET_0 . In spring, the seasonal ET_0 in central and eastern China (i.e. zone III, IV, VI, and VII) was mainly affected by RH. In summer, RH had an important

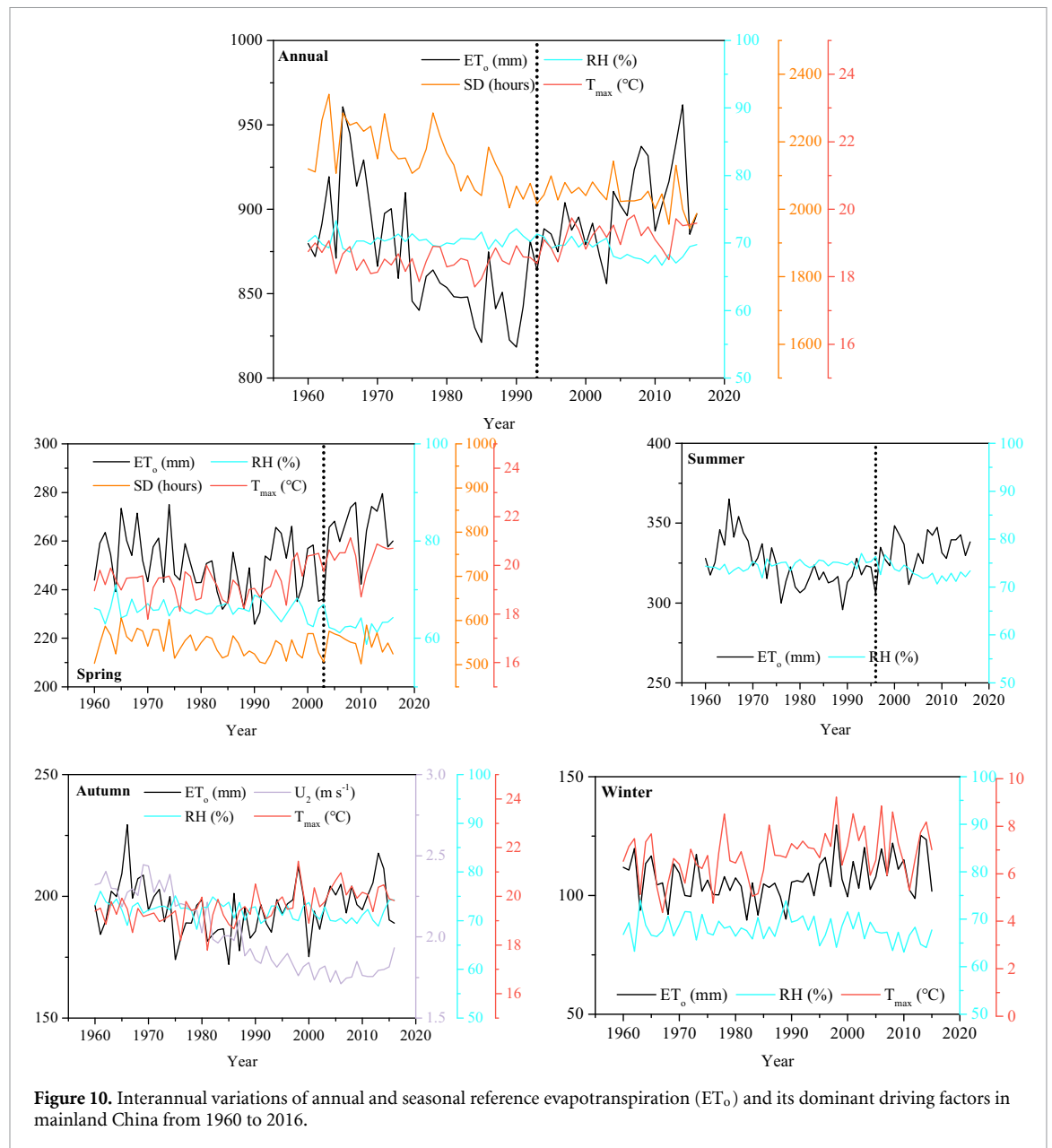


Figure 10. Interannual variations of annual and seasonal reference evapotranspiration (ET_0) and its dominant driving factors in mainland China from 1960 to 2016.

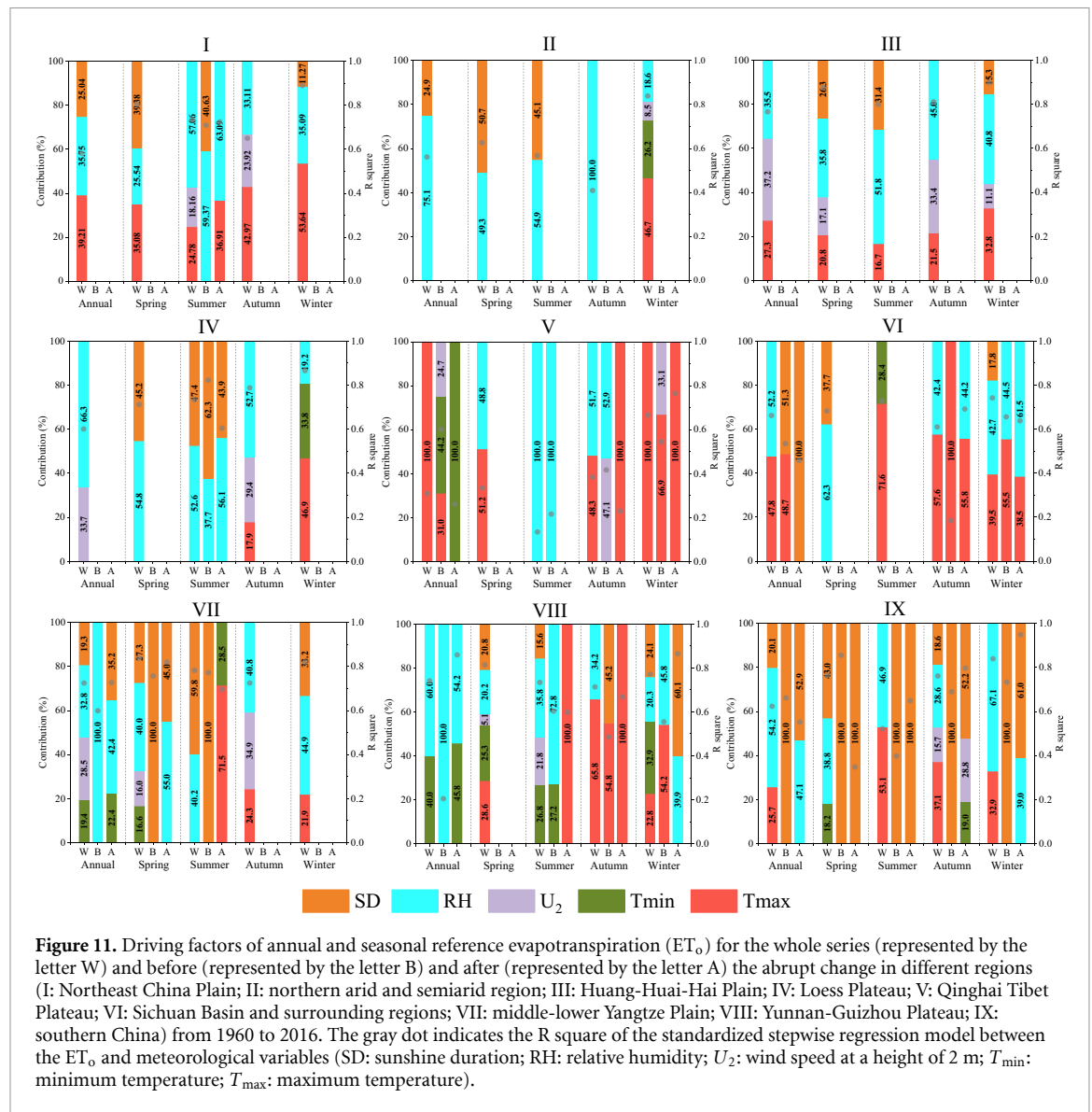
impact on the variability of seasonal ET_0 in northern China (i.e. zone I, II, III, IV, and V). In autumn, the dominant driving factor was RH in northern China, while the T_{max} was the main driver in southern China. However, the main driving factors were approximately opposite in winter compared to that in autumn (figure 11).

Given that the abrupt change mainly occurred in southern China, the analysis of trend change was implemented in zone VI, VII, VIII, and IX. Both before and after abrupt change, the RH and SD were the dominant driving factors of annual ET_0 in zone VII and VIII and zone VII and IX, respectively. After abrupt change, the seasonal ET_0 was mainly influenced by SD in spring and winter in southern China. However, the T_{max} was the dominant driving factor of seasonal ET_0 in summer and autumn after abrupt change. It should be noted that the SD was always the

dominant driver of annual and seasonal ET_0 in zone IX after abrupt change (figure 11).

4. Discussion

The ET_0 is determined by two crucial components: radiative and aerodynamic terms that are comprehensively influenced by climatic factors, such as T , SD, U_2 , and RH (Allen et al 1998, McVicar et al 2007, Dinpashoh et al 2011, Jhajharia et al 2012). In MLC, the high-value regions of annual ET_0 were concentrated in northwestern and southwestern, where the annual ET_0 exceeded 1100 mm. However, northeastern China, the Sichuan Basin, and the middle and lower reaches of the Yangtze River were low-value regions of annual ET_0 , and some of these areas had an annual ET_0 less than 700 mm. Referring to table S1, zones II and IX and zones I and VI showed relatively



high and low annual ET_0 values, respectively. Basically, the district characterized by high air temperature, low atmospheric humidity, strong wind, and long sunshine duration (enhancing the holding capacity of water vapor in the atmosphere, improving the ability of water vapor transport, and meeting the energy requirements of the evaporation surface) had a higher ET_0 , and vice versa.

Trend analysis of the annual ET_0 calculated with high-density meteorological stations in MLC again verified that the abrupt change in the ET_0 sequence induced a downward trend and a subsequent upward trend (Fan et al 2016, Wang et al 2019, Zhang et al 2019). The timing of the abrupt change of the annual ET_0 in the study was 1993, which was slightly different from the results (i.e. 1984 and 1982) by Fan et al (2016) and Wang et al (2017) but similar or identical to the results (i.e. 1990s and 1993) by Wang et al (2019) and Zhang et al (2019), respectively. In the subregions, Jiang et al (2019) indicated that the abrupt change point for ET_0 series occurred in 1996

in Southwest China, which was basically consistent with the result (1997) of abrupt change for zone VIII in the study. In addition, there had few abrupt change of the ET_0 sequence by the Pettitt test in northern China. However, the abrupt change of ET_0 has been detected in some basins or provinces in northern China (Zuo et al 2012, Lv et al 2016, Li et al 2017). The difference of abrupt change point among the relevant studies is principally induced by four aspects that are the calculation procedure of ET_0 , the study area, data source, and the detection method of abrupt change. Compared to the original FAO 56 Penman–Monteith equation, using the corrected R_{ns} and R_{nl} procedure can obtain more accurate ET_0 (Yin et al 2008, Xiao and Kong 2021). In addition, the difference in the aspects of the study area and data source (grids or sites, the quantities of meteorological stations) can also cause the disparity of ET_0 . Furthermore, a series of methods can be adopted to detect the abrupt change of ET_0 sequence, such as Mann–Kendall test (Yang and Tian 2009, Zhao et al 2014,

Fang *et al* 2016), Pettitt (Wang *et al* 2016, 2017), moving *t*-test (MTT) (Lv *et al* 2016, Wu *et al* 2019), cumulative sum (CUSUM) (Lv *et al* 2016, Wang *et al* 2017), Gramer's test (Jiang *et al* 2019), *et al*. And different test methods may present distinct results of abrupt change.

The driving factors of ET_o are determined by two aspects: the sensitivity of ET_o to parameters and the degree of variability of these parameters (Zhao *et al* 2020). Local sensitivity analysis methods, such as partial derivatives, have been widely employed to detect the sensitivity of ET_o to several climatic elements because of the simplicity of the algorithm in China (Huo *et al* 2013, Fan *et al* 2016, She *et al* 2017, Jiang *et al* 2019, Wang *et al* 2019, Zhao *et al* 2020). Nevertheless, a shortcoming of the local approach is that the effect of the variation in a factor on the dependent variable does not include its interactions with other factors. Therefore, a global method named the extended Fourier amplitude sensitivity test (eFAST) (Saltelli *et al* 1999, 2005) was adopted to analyze the first-order sensitivity (single effect) and total sensitivity (mutual effect) of 10 parameters to ET_o . The most sensitive factors were the T_{max} and RH, followed by the U_2 and T_{min} . In contrast, the sensitivities of SD and other parameters were quite small (figure S3). Fan *et al* (2016), Wang *et al* (2019) and Zhao *et al* (2020) also indicated that the RH and T_{max} presented similar high sensitivities.

Although the sensitivities of SD to ET_o were relatively low, the very significant downward trend ($-68.63 \text{ h decade}^{-1}$) of SD indicated that the annual ET_o decreased by $21.2 \text{ mm decade}^{-1}$ from 1960 to 1993 (figure S4). This so-called phenomenon of 'dimming' was consistent with the analyses by Roderick and Farquhar (2002) and Jahani *et al* (2017). After 1993, however, the decreasing trends of SD were relatively weak, and simultaneously, the annual ET_o increased by $21.1 \text{ mm decade}^{-1}$ as the decreasing RH which induced an increase in the vapor pressure deficit of the atmosphere (figure S4). Moreover, the RH and/or T_{max} , as dominant factors, always had a crucial effect on the annual and seasonal pattern of ET_o in most parts of China. The increase in ET_o may intensify the hydrological cycle in humid southern China and exacerbate the drought risk and pressure on water resources in the arid and semiarid regions of northern China. The result about trend change and driving factors of ET_o are expected to serve as a reference for the evaluation of crop water demand, drought risk assessment and water resource allocation in MLC.

5. Conclusions

Coefficients 'a' and 'b' in the Angstrom–Prescott model were lower and higher than the reference values (i.e. 0.25 and 0.50) of FAO paper 56, respectively, in most parts of China, except for a small area of

western and northeastern China. The temporal variations in the two parameters were all characterized by annual and seasonal patterns that first decreased and then increased from 1960 to 2016, but they had different change points. In addition, the Xiao's method to estimate R_{nl} can greatly improve the accuracy of ET_o .

In MLC, the multiyear average annual ET_o was from 538.8 to 1559.8 mm, with a high-value region exceeding 1100 mm located in the plateau and desert areas of western and northwestern China and a low-value region below 700 mm located in northeastern China and near the Sichuan Basin. Moreover, the seasonal ET_o was highest in summer, followed by that in spring, autumn, and winter. The spatial distribution of seasonal ET_o was roughly similar to that of annual ET_o , except for that in winter when ET_o was low in northern China and high in southern China.

An abrupt change point that appeared in 1993 separated the annual ET_o sequence into two segments: a decreasing interval with a slope of $21.2 \text{ mm decade}^{-1}$ and an increasing interval with a slope of $21.1 \text{ mm decade}^{-1}$ in MLC. Except for Qinghai Tibet Plateau, few abrupt change points of the ET_o sequences have been detected in northern China. Although the abrupt change of annual ET_o sequences occurred in most of the southern China, the timing of the abrupt change was not consistent. However, the abrupt change of the seasonal ET_o in southern China generally occurred in approximately 1995, especially in autumn and winter. In MLC, the driving factors of annual ET_o was SD before 1993 and RH after 1993. Basically, the variation in the annual and seasonal ET_o was mostly controlled by RH and/or T_{max} in most parts of China.

Data availability statement

The data generated and/or analysed during the current study are not publicly available for legal/ethical reasons but are available from the corresponding author on reasonable request.

Acknowledgments

This work was supported by the National Key Research and Development Program of China (Grant No. 2019YFC1510205), the National Natural Science Foundation of China (Grant No. 42075193) and the Fundamental Research Fund (Grant No. 2019Z010).

ORCID iD

Dong Wu  <https://orcid.org/0000-0002-3202-255X>

References

- Allen R G, Pereira L S, Raes D and Smith M 1998 Crop evapotranspiration: guidelines for computing crop water requirements Irrigation and Drainage Paper No. 56 (Rome: United Nations Food and Agriculture)

- Anderson M C, Hain C, Wardlow B, Pimstein A, Mecikalski J R and Kustas W P 2011 Evaluation of drought indices based on thermal remote sensing of evapotranspiration over the continental United States *J. Clim.* **24** 2025–44
- Arnell N and Liu C-Z 2001 *Hydrology and Water Resources, in Climate Change 2001: Impacts, Adaptation, and Vulnerability—Contribution of Working Group II to the Third Assessment Report of the Intergovernmental Panel on Climate Change* (New York: Cambridge University Press)
- Ayantobo O O, Li Y, Song S and Yao N 2017 Spatial comparability of drought characteristics and related return periods in mainland China over 1961–2013 *J. Hydrol.* **550** 549–67
- Bastiaanssen W G M, Menenti M, Feddes R A and Holtslag A A M 1998 A remote sensing surface energy balance algorithm for land (SEBAL) 1 Formulation *J. Hydrol.* **212–213** 198–212
- Chattopadhyay N and Hulme M 1997 Evaporation and potential evapotranspiration in India under conditions of recent and future climate change *Agric. For. Meteorol.* **87** 55–73
- Dinpashoh Y, Jhajharia D, Fakheri-Fard A, Singh V P and Kahya E 2011 Trends in reference crop evapotranspiration over Iran *J. Hydrol.* **399** 422–33
- Doorenbos J and Pruitt W O 1977 Guidelines for predicting crop water requirements Irrigation and Drainage Paper 24 (Rome: Food and Agriculture Organization of the United Nations) p 179
- Fan J, Wu L, Zhang F, Xiang Y and Zheng J 2016 Climate change effects on reference evapotranspiration across different climatic zones of China during 1956–2015 *J. Hydrol.* **542** 923–37
- Fan Z-X and Thomas A 2018 Decadal changes of reference crop evapotranspiration attribution: spatial and temporal variability over China 1960–2011 *J. Hydrol.* **560** 461–70
- Fang S, Qi Y, Han G, Li Q and Zhou G 2016 Changing trends and abrupt features of extreme temperature in mainland China during 1960–2010 *Atmosphere* **7** 979–1000
- Gao Z, He J, Dong K and Li X 2017 Trends in reference evapotranspiration and their causative factors in the West Liao River basin, China *Agric. For. Meteorol.* **232** 106–17
- Gu X, Zhang Q, Singh V P and Shi P 2017 Changes in magnitude and frequency of heavy precipitation across China and its potential links to summer temperature *J. Hydrol.* **547** 718–31
- Hanasaki N, Kanae S, Oki T, Masuda K, Motoya K, Shirakawa N, Shen Y and Tanaka K 2008 An integrated model for the assessment of global water resources-part 2: applications and assessments *Hydrol. Earth Syst. Sci.* **12** 1027–37
- Hirsch R M and Slack J R 1984 A nonparametric trend test for seasonal data with serial dependence *Water Resour. Res.* **20** 727–32
- Hobbins M T and Ramirez J A 2004 Trends in pan evaporation and actual evapotranspiration across the conterminous U.S.: paradoxical or complementary? *Geophys. Res. Lett.* **31** L13503
- Huo Z, Dai X, Feng S, Kang S and Huang G 2013 Effect of climate change on reference evapotranspiration and aridity index in arid region of China *J. Hydrol.* **492** 24–34
- Itenfisu D, Elliott R L, Allen R G and Walter I A 2003 Comparison of reference evapotranspiration calculations as part of the ASCE standardization effort *J. Irrig. Drain. Eng.* **129** 440–8
- Jahani B, Dinpashoh Y and Wild M 2017 Dimming in Iran since the 2000s and the potential underlying causes *Int. J. Climatol.* **38** 1543–59
- Jhajharia D, Dinpashoh Y, Kahya E, Singh V P and Ahmad F-F 2012 Trends in reference evapotranspiration in the humid region of northeast India *Hydrol. Pross.* **26** 421–35
- Jiang S, Liang C, Cui N, Zhao L, Du T, Hu X, Feng Y, Guan J and Feng Y 2019 Impacts of climatic variables on reference evapotranspiration during growing season in Southwest China *Agr. Water Manage.* **216** 365–78
- Li Y, Yao N and Chau H W 2017 Influences of removing linear and nonlinear trends from climatic variables on temporal variations of annual reference crop evapotranspiration in Xinjiang, China *Sci. Total Environ.* **592** 680–92
- Liang L, Li Q and Liu Q 2010 Temporal variation of reference evapotranspiration during 1961–2015 in the Taer River basin of Northeast China *Agric. For. Meteorol.* **150** 298–306
- Lv M-Q, Chen J-L, Mirza Z A, Chen C-D, Wen Z-F, Jiang Y, Ma M-H and Wu S-J 2016 Spatial distribution and temporal variation of reference evapotranspiration in the three Gorges Reservoir area during 1960–2013 *Int. J. Climatol.* **36** 4497–511
- McVicar T R et al 2012 Global review and synthesis of trends in observed terrestrial near-surface wind speeds: implications for evaporation *J. Hydrol.* **416–417** 182–205
- McVicar T R, Van Niel T G, Li L, Hutchinson M F, Mu X and Liu Z 2007 Spatially distributing monthly reference evapotranspiration and pan evaporation considering topographic influences *J. Hydrol.* **338** 196–200
- National Standard of People's Republic of China, GB/T35230-2017 2017 Specifications for surface meteorological observation-evaporation
- Norman J M, Kustas W P and Humes K S 1995 Source approach for estimating soil and vegetation energy fluxes observations of directional radiometric surface temperature *Agric. For. Meteorol.* **77** 263–93
- Papaioannou G, Kitsara G and Athanasatos S 2011 Impact of global and brightening on reference evapotranspiration in Greece *J. Geophys. Res.* **116** D09107
- Penman H L 1948 Natural evaporation from open water, bare soil and grass *Proc. R. Soc.* **193** 120–45
- Pettitt A N 1979 A non-parametric approach to the change-point problem *Appl. Stat.* **28** 126–35
- Rayner D P 2007 Wind run changes: the dominant factor affecting pan evaporation trends in Australia *J. Clim.* **20** 3379–94
- Roderick M L and Farquhar G D 2002 The cause of decreased pan evaporation over the past 50 years *Science* **298** 1410–1
- Saltelli A, Ratto M, Tarantola S and Campolongo F 2005 Sensitivity analysis for chemical models *Chem. Rev.* **105** 2811–27
- Saltelli A, Tarantola S and Chan K P S 1999 A quantitative model-independent method for global sensitivity analysis of model output *Technometrics* **44** 39–56
- Sen P K 1968 Estimates of the regression coefficient based on Kendall's tau *J. Am. Stat. Assoc.* **63** 1379–89
- She D, Xia J and Zhang Y 2017 Changes in reference evapotranspiration and its driving factors in the middle reaches of Yellow River Basin, China *Sci. Total Environ.* **607–608** 1151–62
- Soubie R, Heinesch B, Granier A, Aubinet M and Vincke C 2016 Evapotranspiration assessment of a mixed temperate forest by four methods: Eddy covariance, soil water budget, analytical and model *Agric. For. Meteorol.* **228** 191–204
- Thomas A 2000 Spatial and temporal characteristics of potential evapotranspiration trends over China *Int. J. Climatol.* **20** 381–96
- Villarini G, Smith J A, Serinaldi F, Ntelekos A A and Schwarz U 2012 Analyses of extreme flooding in Austria over the period 1951–2006 *Int. J. Climatol.* **32** 1178–92
- Wang Q, Wang J, Zhao Y, Li H, Zhai J, Yu Z and Zhang S 2016 Reference evapotranspiration trends from 1980 to 2012 and their attribution to meteorological drivers in the three-river source region, China *Int. J. Climatol.* **36** 3759–69
- Wang Z, Xie P, Lai C, Chen X, Wu X, Zeng Z and Li J 2017 Spatiotemporal variability of reference evapotranspiration and contributing climatic factors in China during 1961–2013 *J. Hydrol.* **544** 97–108
- Wang Z, Ye A, Wang L, Liu K and Cheng L 2019 Spatial and temporal characteristics of reference evapotranspiration and its climatic driving factors over China from 1979–2015 *Agric. Water Manage.* **213** 1096–108
- Wu D, Fang S, Li X, He D, Zhu Y, Yang Z, Xu J and Wu Y 2019 Spatial-temporal variation in irrigation water requirement for the winter wheat-summer maize rotation system since the 1980s on the North China Plain *Agric. Water Manage.* **214** 78–86

- Xiang K, Li Y, Horton R and Feng H 2020 Similarity and difference of potential evapotranspiration and reference crop evapotranspiration—a review *Agric. Water Manage.* **232** 1–16
- Xiao M and Kong D 2021 Improvement in the estimation of daily net surface radiation in China *J. Irrig. Drain. Eng.* **147** 04021002
- Xu C, Gong L, Jiang T, Chen D and Singh V P 2006 Analysis of spatial distribution and temporal trend of reference evapotranspiration and pan evaporation in Changjiang (Yangtze River) catchment *J. Hydrol.* **327** 81–93
- Yang X, Chen Y, Pacenka S, Gao W, Ma L, Wang G, Yan P, Sui P and Steenhuis T S 2015 Effect of diversified crop rotations on groundwater levels and crop water productivity in the North China Plain *J. Hydrol.* **522** 428–38
- Yang Y and Tian F 2009 Abrupt change of runoff and its major driving factors in Haihe River catchment *China J. Hydrol.* **374** 373–83
- Yang Y and Yang D 2012 Climatic factors influencing changing pan evaporation across China from 1961 to 2001 *J. Hydrol.* **414–415** 184–93
- Yee M S, Pauwels V R N, Daly E, Beringer J, Rüdiger C, McCabe M F and Walker J P 2015 A comparison of optical and microwave scintillometers with eddy covariance derived surface heat fluxes *Agric. For. Meteorol.* **213** 226–39
- Yin Y, Wu S, Zheng D and Yang Q 2008 Radiation calibration of FAO56 Penman-Monteith model to estimate reference crop evapotranspiration in China *Agric. Water Manage.* **95** 77–84
- Yue S and Wang C 2002 Application of prewhitening to eliminate the influence of serial correlation on the Mann-Kendall test *Water Resour. Res.* **38** 4-1–4-7
- Zhang L, Traore S, Cui Y, Luo Y, Zhu G, Liu B, Fipps G, Karthikeyan R and Singh V 2019 Assessment of spatiotemporal variability of reference evapotranspiration and controlling climate factors over decades in China using geospatial techniques *Agric. Water Manage.* **213** 499–511
- Zhao G, Tian P, Mu X, Jiao J, Wang F and Gao P 2014 Quantifying the impact of climate variability and human activities on streamflow in the middle reaches of the Yellow River, China *J. Hydrol.* **519** 387–98
- Zhao Z, Wang H, Wang C, Li W, Chen H and Deng C 2020 Changes in reference evapotranspiration over Northwest China from 1957 to 2018: variation characteristics, cause analysis and relationships with atmospheric circulation *Agric. Water Manage.* **231** 105958
- Zuo D, Xu Z, Yang H and Liu X 2012 Spatiotemporal variations and abrupt changes of potential evapotranspiration and its sensitivity to key meteorological variables in the Wei River basin *China Hydrol. Process.* **26** 1149–60